Available online at www.sciencedirect.com
SCIENCE DIRECT®
Coastal Engineering xx (2004) xxx–xxx
Coastal Engineering
An International Journal for Coastal, Harbour and Offshore Engineers
www.elsevier.com/locate/coastaleng

Estimates of winter currents on the Israeli continental shelf

D. Kunitsa[a], Z. Rosentraub[b], M. Stiassnie[a,*]

[a]Department of Civil and Environmental Engineering, Technion-Israel Institute of Technology, Haifa 32000, Israel
[b]Israel Oceanographic and Limnological Research, Tel Shikmona, Haifa 31080, Israel

Received 14 August 2003; received in revised form 12 July 2004; accepted 24 September 2004

Abstract

A simplified analytical model for continental shelf wind-driven currents is adopted. The calculated results compare favorably with extensive field measurements from two separate sources. The model is used to hindcast the current climatology on the Israeli continental shelf. The maximum northward/southward alongshore currents at 10-m water depth, with a return period of 100 years, are found to be 1.28 and 0.53 m/s, respectively.
© 2004 Published by Elsevier B.V.

Keywords: Coastal currents; Continental shelf currents; Wind-induced current; Israeli coast; Israeli continental shelf

UNCORRECTED PROOF

1. Introduction

The motivation of this study is to provide a clear picture of the winter current regime on the Israeli continental shelf, based on measurements and theory. These currents are needed for the assessment of the ecological and sedimentological impacts of man-made coastal projects. Actual field measurements of currents are scarce, but worldwide data bases of past wind and pressure fields become more available. The latter can be used in conjunction with simple mathematical models to produce synthetic records of continental shelf currents. In turn, these records may serve as input to other numerical studies, including morphodynamics, power plant cooling water recirculation, desalination plant brine recirculation, etc.

The depth over the Israeli continental shelf varies slowly from the shoreline to about 100 m where the continental slope begins. The Israeli shelf is relatively narrow: 20 km at Ashqelon and only 10 km near Atlit, see Figs. 1 and 2.

In the summer of 1987, the Israel Oceanographic and Limnological Research Institute (IOLR) initiated a long-term program of measuring the regime of currents on the Israeli continental shelf and slope. The field measurements consisted of direct current measurements with current meters mounted on subsurface moorings and measurements of bottom pressure at several fixed locations out to a water depth of 120 m.

From 1994, measurements were also made on the continental slope at a water depth of 500 m opposite

* Corresponding author. Tel.: +972 4 8293361.
E-mail address: miky@tx.technion.ac.il (M. Stiassnie).

0378-3839/$ - see front matter © 2004 Published by Elsevier B.V.
doi:10.1016/j.coastaleng.2004.09.004

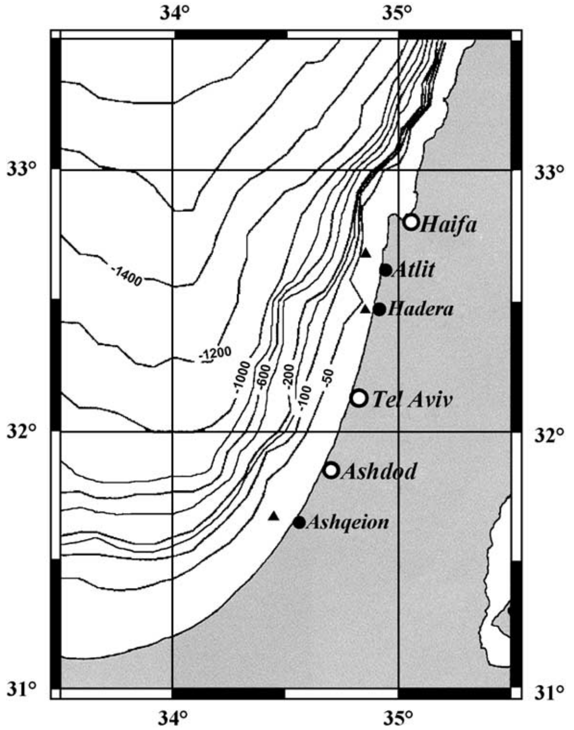

Fig. 1. Current measurements stations (marked by a triangle) on the Israeli continental shelf during the 1987–1994 IOLR project, used in this study. Contour lines show the water depth in meters.

Hadera. In addition, several hydrographic cruises were conducted, during which density cross-sections normal to the coast were sampled. The stations, referred herein, for which some measurements of currents took place between 1987 and 1994, are marked by a triangle in Fig. 1. The main findings of this experimental effort appear in Rosentraub (1992, 1995; both available on request).

From Rosentraub (1992, 1995), one learns that his measurements detected currents directed mainly northward during all seasons, following the bathymetric lines. The alongshore component of the flow dominated the cross-shore component by a factor of four or more, even when both components of the wind stress were of the same order of magnitude. During the winter season, the flow was uniform throughout the water column, and the water density was also approximately uniform in depth, see Fig. 2. In summer, the flow decreased away from the surface due to density gradients. Spectral analysis demonstrated the importance of the local wind in driving the currents. Note that the tidal component in the current is negligible along the Israeli Mediterranean coast.

The continental shelf structure and the measurements allow us to assume that the sea over the shelf is a shallow-water basin limited on one side with a coastline, which, at least locally, is straight. The bathymetry lines in this basin are approximately parallel to the coastline. The water mass during winter periods can be taken as homogeneous, as seen in Fig. 2.

In the following section, we present and calibrate a simplified mathematical model for the coastal currents. The overall comparison of the calculated results with the IOLR measurements and with more recent Oceana measurements is presented in Sections 3 and 4, respectively. A hindcasted current climatology for the Israeli Mediterranean continental shelf is calculated and presented in Section 5. Conclusions are drawn and limitations are discussed in Section 6.

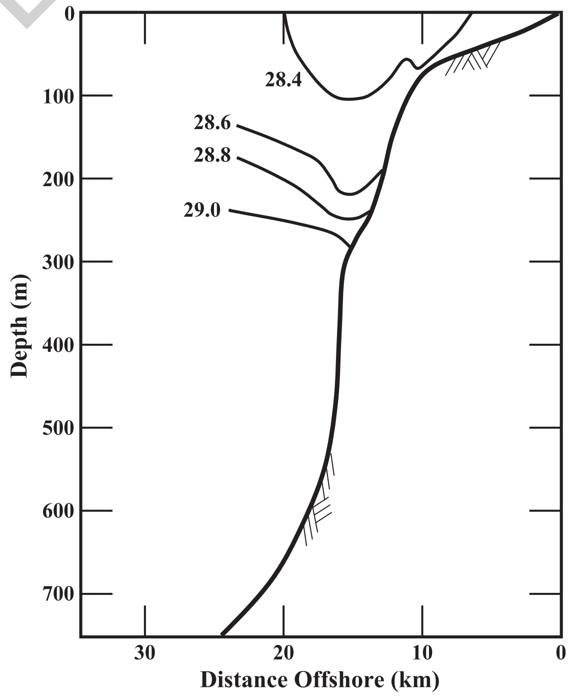

Fig. 2. Typical winter density cross-section on the shelf and slope off Atlit (from Rosentraub, 1995).

UNCORRECTED PROOF

ARTICLE IN PRESS

2. Simplified theory and calibration

2.1. Simplified theory

Following Lentz and Winant (1986) and Hickey et al. (2003), we adopt the framework of linearized shallow water theory, for which the equations of motion and equation of continuity are given by

$$\frac{\partial u}{\partial t} - fv = -g\left(\frac{\partial \eta}{\partial x} + \frac{\partial \eta_a}{\partial x}\right) - \frac{ru}{h} + \frac{X}{h} \tag{1}$$

$$\frac{\partial v}{\partial t} + fu = -g\left(\frac{\partial \eta}{\partial y} + \frac{\partial \eta_a}{\partial y}\right) - \frac{rv}{h} + \frac{Y}{h} \tag{2}$$

$$\frac{\partial}{\partial x}(hu) + \frac{\partial}{\partial y}(hv) = -\frac{\partial \eta}{\partial t} \tag{3}$$

u and v are the depth averaged components of velocity in the x and y direction, respectively, η is the free-surface elevation, and η_a is the atmospheric pressure to the specific weight of the water ratio. f is the Coriolis parameter, assumed to be constant in the domain of interest. X and Y are the x and y components of the wind stress divided by the density of the water; they are assumed to be functions of time t only. r is a constant friction coefficient, and h is the water depth.

We are seeking solutions to the above system of equations over a simplified continental shelf for which $h=h(y)$. The coordinate x is along the shoreline, and y points seawards. We denote the shelf width by l, so that the problem has to be solved for $y \in (0,l)$.

Because the driving forces, the deep-water surface elevation η at $y=l$, and the geometry are assumed to be independent of the alongshore coordinate, we set all the x derivatives in Eqs. (1–3) to zero; except the alongshore atmospheric pressure gradient $\partial\eta_a/\partial x$, which is only a function of time. Based on the measurements, we also assume that vu, which enables a further simplification of the system, which reduces to decoupled equations

$$\frac{\partial u}{\partial t} + \frac{ru}{h} = \frac{X}{h} - g\frac{\partial \eta_a}{\partial x} \tag{4}$$

$$g\frac{\partial \eta}{\partial y} = -fu + \frac{Y}{h} - g\frac{\partial \eta_a}{\partial y} \tag{5}$$

$$\frac{\partial}{\partial y}(hv) = -\frac{\partial \eta}{\partial t} \tag{6}$$

Eq. (4) has the following solution

$$u(y,t) = h^{-1}\int_0^t e^{\frac{r}{h}(\tau - t)}\tilde{X}(\tau)\mathrm{d}\tau \tag{7}$$

where

$$\tilde{X}(\tau) = X(\tau) - gh\frac{\partial \eta_a(\tau)}{\partial x} \tag{8}$$

In Eq. (7), it was assumed that the induced flow starts from rest at $t=0$. Eq. (7), for constant $\tilde{X}$, leads to the same result as Eq. (14a) in Brink (1998).

Once $u(y,t)$ is known, Eq. (5) gives

$$\eta(y,t) = -\frac{1}{g}\int_y^l\left[\frac{\tilde{Y}(t)}{h(\zeta)} - fu(\zeta,t)\right]\mathrm{d}\zeta \tag{9}$$

where the boundary condition $\eta(l,t)=0$ has been imposed. Here, similar to Eq. (8)

$$\tilde{Y}(\tau) = Y(\tau) - gh\frac{\partial \eta_a(\tau)}{\partial y} \tag{10}$$

Substituting Eq. (9) into Eq. (6) and integrating with respect to y yields

$$v(y,t) = -\frac{1}{h}\int_0^y \frac{\partial \eta(\zeta,t)}{\partial t}\mathrm{d}\zeta \tag{11}$$

where the coastal no-flux $hv|_{y=0}=0$ boundary condition was taken into account.

It should be made clear that by using the above model, we implicitly assume that the currents are primarily a result of local wind and atmospheric pressure-gradient forcing, rather than a manifestation of a collection of northward propagating shelf waves.

Table 1
Series of measured current velocities on the Israeli continental shelf used in this study

Number	Period	Location	D (km)	h_m (m)	h (m)
Series 1	04.12.87–17.04.88	Atlit	9.4	37	90
Series 2	15.01.91–31.03.91	Ashqelon	2.2	18	26
Series 3	15.01.91–31.03.91	Hadera	2.0	20	25
Series 4	31.10.91–27.01.92	Ashqelon	2.2	18	26
Series 5	27.11.93–03.04.94	Hadera	2.0	19	27

D—offshore distance, h_m—depth of current meter, h—water depth.

UNCORRECTED PROOF

ARTICLE IN PRESS

2.2. Bottom friction assessment

To close the model, it was necessary to compare current velocities calculated from actual wind data with results of current velocity measurements for the same period of time. Five time series of winter current velocities on the Israeli continental shelf were provided by IOLR (Table 1). These time series included hourly components of current velocity. The wind and atmospheric pressure data for these periods, in 6-h intervals, were available from the NCEP/NCAR database described in Section 5.

Components of the wind shear stress acting on the water surface (X,Y) were calculated in this study as

$$(X,Y) = k|\boldsymbol{W}|\boldsymbol{W}, \tag{12}$$

where $\boldsymbol{W}$ the wind speed vector at a reference elevation of 10 m, and k a dimensionless friction factor of order 10^{-6}. k was taken from one of the more widely used empirical expressions

$$k = \begin{cases} 1.2\times10^{-6}, |\boldsymbol{W}|\leq W_c \\ 1.2\times10^{-6} + 2.25\times10^{-6}(1 - W_c/|\boldsymbol{W}|), \quad |\boldsymbol{W}|>W_c \end{cases} \tag{13}$$

where W_c=5.6 m/s, Dean and Dalrymple (1991).

Different studies use r within a wide range, varying from 10^{-4} to 10^{-3} m/s, see Csanaday (1978). The methodology we have used consists of the following steps. First, we have calculated hindcasted currents for all five series related to those of Table 1, for different values of r. Second, we formed for each r one long time series, by placing the above five series one after the other. The same procedure was followed for the measured currents. Third, for each of the rs, as well as for the measurements, we calculated five quantities:

1. The percentage of time for which northern currents occur, denoted by % (+).
2. The mean northern current $\bar{u}$ (+).
3. The mean southern current $\bar{u}$ (−).
4. The variance of the northern currents σ (+).
5. The variance of the southern currents σ (−).

Table 2
The influence of different values of bottom friction, see text

r (m/s)	% $(+)_{h/m}$	$\bar{u}\ (+)_{h/m}$	$\bar{u}\ (-)_{h/m}$	$\sigma\ (+)_{h/m}$	$\sigma\ (-)_{h/m}$
2.0×10^{-4}	1.02	1.09	1.13	1.17	0.96
2.2×10^{-4}	0.99	1.03	1.01	1.08	0.77
2.4×10^{-4}	0.98	0.94	0.85	0.99	0.67

Last, we calculated the ratios (subscript h/m) between the above five values as calculated from the hindcast (subscript h), to their counterparts calculated from the measurements (subscript m); that is, $\bar{u}\ (+)_{h/m}$ $=\bar{u}\ (+)_h/\bar{u}\ (+)_m$,. . .These ratios are presented in Table 2 for three different values of r.

Values of r outside the range given in Table 2 were checked and found less favorable. By inspecting Table 2, we have decided to choose r=2.2×10^{-4} m/s as most appropriate for the Israeli coast.

3. Correlation between measurements and theory

The hindcasted current velocities for all five time series together with the results of current measurements are presented in Fig. 3. The correlation coefficients between hindcasted u_h and measured u_m current velocity time series, defined as

$$c_r(u_h, u_m) = \frac{\sum_{i=1}^{n}\left[\left(u_h^i - \bar{u}_h\right)\left(u_m^i - \bar{u}_m\right)\right]}{\sqrt{\sum_{i=1}^{n}\left(u_h^i - \bar{u}_h\right)^2 \sum_{i=1}^{n}\left(u_m^i - \bar{u}_m\right)^2}}, \tag{14}$$

where n is the number of points in the time series, which varies from 0.59 (Series 3) to 0.84 (Series 5)[1]. At the same time we note some underestimation in hindcasted values of the Southern current.

As it follows from Eq. (4), the influence of the alongshore atmospheric pressure gradient strongly depends on the water depth. For a shallow depth, its influence is relatively weak, whereas, for a large depth, it can be as important as the wind stress forcing. For example, the addition of atmospheric pressure gradient to the source function in Eq. (8) changed the correlation coefficient for Series 5 (h=27 m) from 0.78 to 0.84. At the same time, the same

[1] These values are highly significant, if one takes into account $n/60$ degrees of freedom for each series, reflecting an estimated time scale for independence of measurements of 2.5 days, see Allen and Kundu (1978).

UNCORRECTED PROOF

ARTICLE IN PRESS

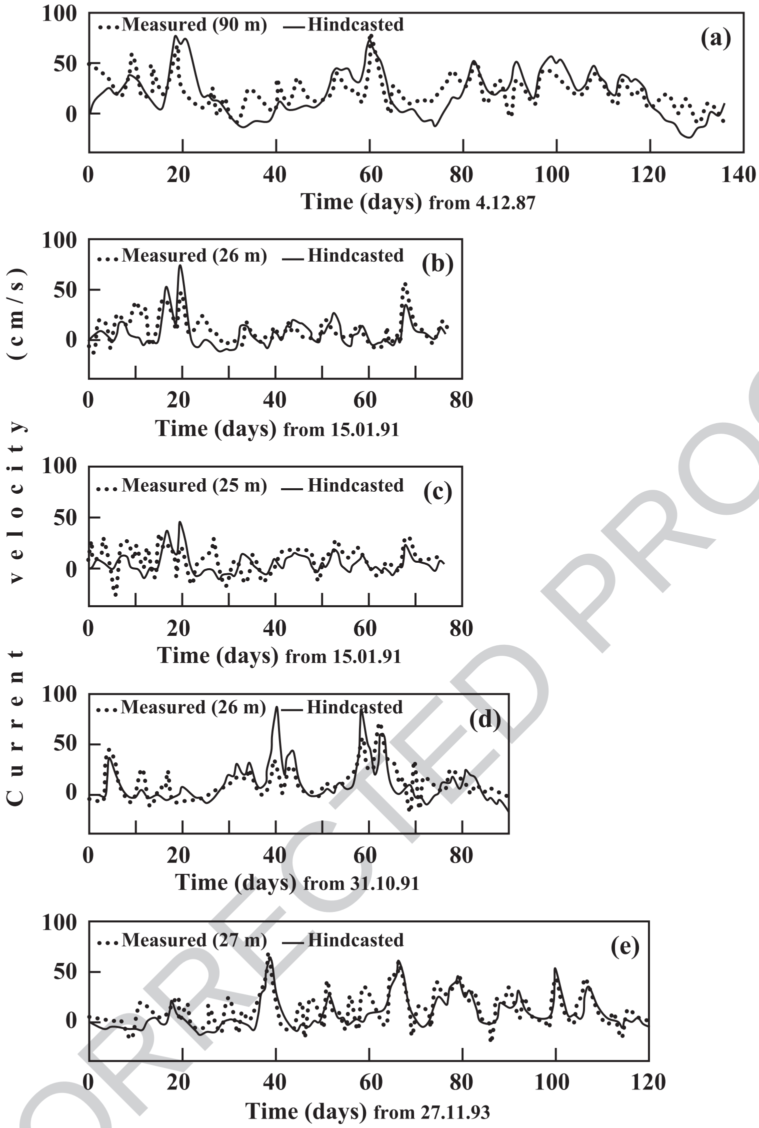

Fig. 3. Calculated and measured alongshore components of current velocity for (a) Series 1 (c_r=0.71), (b) Series 2 (c_r=0.68), (c) Series 3 (c_r=0.59), (d) Series 4 (c_r=0.73), and (e) Series 5 (c_r=0.84).

addition changed the correlation coefficient for Series 1 (h=90 m) from 0.56 to 0.71.

Statistical analysis of the five measured time series of the northern alongshore component of current velocity yields reasonable agreement with the exponential probability density distribution

$$f(u) = \frac{1}{\mu} e^{-\frac{u}{\mu}} \qquad (15)$$

where μ is the distribution parameter (Fig. 4). The main feature of this distribution is that its mean value, as well as its variance, is given by the distribution parameter μ. In Fig. 4, this parameter, obtained by the maximum likelihood method for each time series, is compared with the mean value of the same series. Visual inspection reveals good agreement between the histograms and the calculated probability density functions, except for Series 1,

UNCORRECTED PROOF

ARTICLE IN PRESS

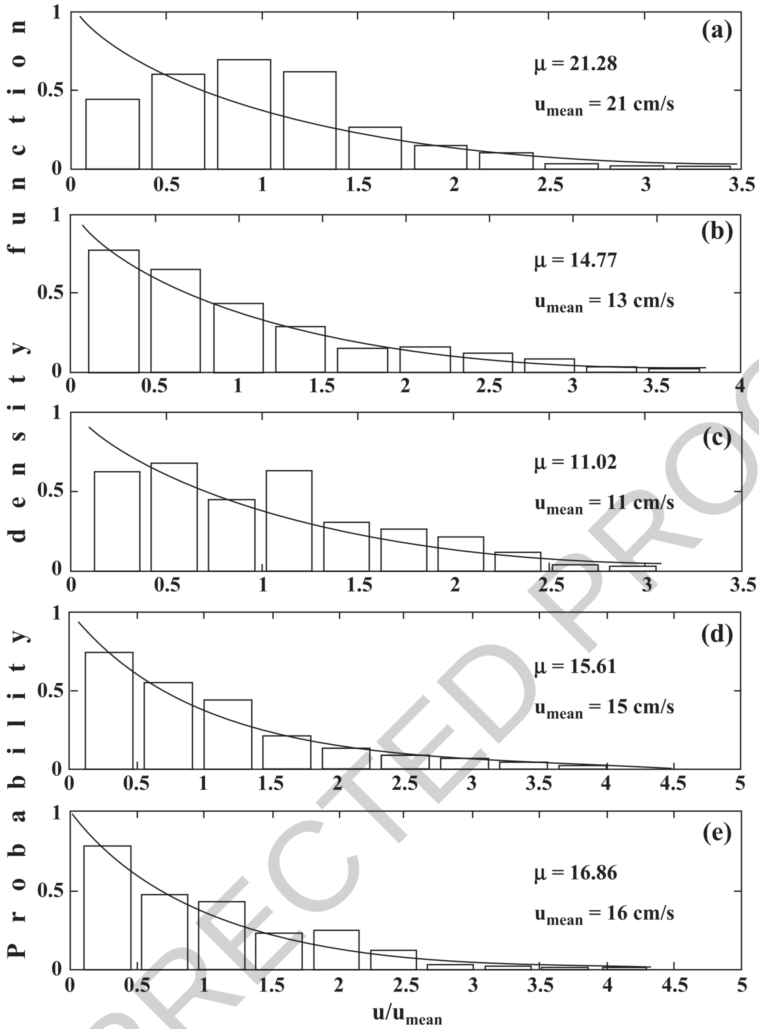

Fig. 4. Distribution of measured alongshore components of current velocity for northern currents (histogram) and calculated probability density functions of the exponential distribution (solid line) for (a) Series 1, (b) Series 2, (c) Series 3, (d) Series 4, and (e) Series 5.

despite good agreement between μ and $\bar{u}$. Some explanation is found in Table 3, where $\bar{u}$ (+) and σ (+) values are always rather similar, except the first case describing the same Atlit time series. The measurements in Atlit are in much deeper water than those in Ashkelon and Hadera, 90 m compared to 26 m. From Eq. (1), it is clear that in the deep water, the effect of alongshore sea level gradient (which we have neglected) is more profound. Good agreement between μ and $\bar{u}$ allows one to use the mean value as the main parameter for the series statistics, which are nearly exponentially distributed.

4. Model verification using independent measurements

The model performance was verified using an independent set of measured current velocities. These measurements were conducted in the region of Ashdod port by Oceana, for the Ports and Railways Authority of Israel.

Oceana has been commissioned to perform current measurements above the bottom (about 1 m) off Ashdod breakwater at two water depths: 15 and 23.5 m. Measurements were carried out during

UNCORRECTED PROOF

ARTICLE IN PRESS

Table 3
Statistical parameters of measured and hindcasted time series of the alongshore component of current velocity for the northern (+) and southern (−) directions

Series		+ (%)	− (%)	$\bar{u}$ (+) (cm/s)	$\bar{u}$ (−) (cm/s)	σ (+) (cm/s)	σ (−) (cm/s)
Atlit	Hindcasted	89	11	20	4	11	3
04.12.87–17.04.88	Measured	91	9	21	5	12	4
Ashqelon	Hindcasted	74	26	11	4	11	2
15.01.91–31.03.91	Measured	72	28	13	4	12	3
Hadera	Hindcasted	70	30	9	6	6	3
15.01.91–31.03.91	Measured	73	27	11	7	7	5
Ashqelon	Hindcasted	65	35	17	4	16	3
31.10.91–27.01.92	Measured	68	32	15	5	13	4
Hadera	Hindcasted	70	30	15	4	12	3
27.11.93–03.04.94	Measured	73	27	16	5	13	5

$\bar{u}$ is the averaged velocity and σ is its variance.

the 3-year period between May 1995 and July 1998 (Kit, 1999).

We used the hourly averaged measured current velocities for three winter periods: 1995–1996, 1996–1997, and 1997–1998. These currents were compared to the currents calculated using our simplified analytical model based on the wind and the atmospheric pressure input for the same periods of time. The wind and the atmospheric pressure data from the NOAA database, used in this work, was available to us only until December, 1997. The calculated currents for January–March, 1998, were based on the wind measured at Ashdod port. The influence of the atmospheric pressure gradient in this last case was neglected.

The currents were calculated for two water depths: 15 and 23.5 m, according to measured data. The calculations were proceeded continuously for entire winter periods (November–March), and the results were compared to measured data, when and where it was available.

The results of this comparison are presented in Figs. 5 and 6). There is a good agreement between hindcasted and measured current velocities at both water depths. In the last series (Fig. 6), based on the wind measured in Ashdod, we can also see reasonable agreement in southern current velocities.

5. Hindcast of current climatology

5.1. Calculation of winter currents for a 40-year period

The wind and pressure data for the model calibration described in Section 2 were made available by NOAA in the NCEP/NCAR database. This database was created as a result of the NCEP/NCAR CDAS/Reanalysis Project—a joint project between the National Centers for Environmental Prediction (NCEP, formerly “NMC”) and the National Center for Atmospheric Research (NCAR). The goal of this joint effort was to produce new atmospheric analyses using historical data (1957 onwards), as well as to produce analyses of current atmospheric state (Climate Data Assimilation System, CDAS; Jenne and Woollen, 1994; Kalnay et al., 1996).

As a result of this project, different meteorological data for the last 40-year period is available in gridded binary (GRIB) form—the standard WMO format for the storage of weather product information.

In this study, we used maps of two components of the wind speed at 10 m level with 6-h time intervals and horizontal spacing of 1°52′30″ in longitude and 1°54′18″ in latitude. Our previous experience of using these data led us to increase the wind speed by 25% (Kushnir et al., 2000). Similar findings regarding wind speed over the Mediterranean Sea are reported by Large and Yeager (2004). The horizontal spacing of the atmospheric pressure maps was more coarse—2°30′ in longitude and in latitude.

Current velocities were calculated separately for each month of the winter period (November–March) and each year of the 40 years (1958–1997). The calculation was carried out for three depths—10, 20, and 50 m. To check the trend for shallower depths, we calculated current velocity also for a depth of 1 m (which is well within the breaker zone where wave induced alongshore current dominates).

As a result of this calculation, 200 time series for every depth (five winter months for each of the years 1958–1997) were obtained.

5.2. Current statistics for the 40-year period

Statistical parameters (mean and maximum values of the alongshore component of current velocity for

UNCORRECTED PROOF

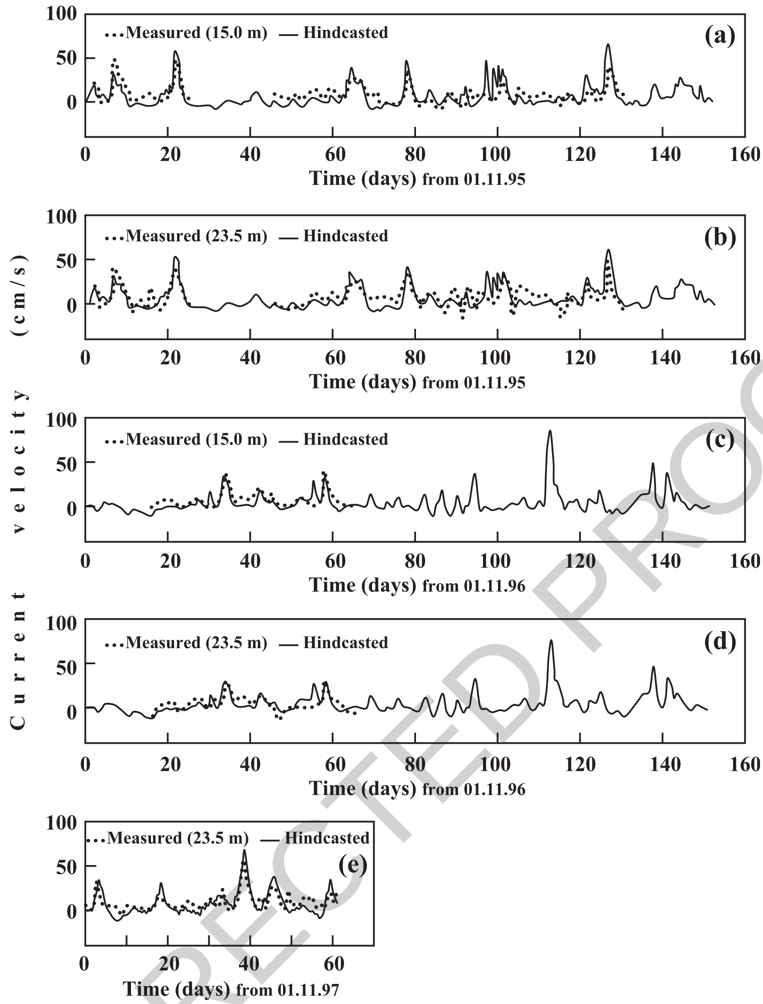

Fig. 5. Calculated and measured alongshore components of current velocity near Ashdod port: (a) for the 11,1995–03,1996 period at 15.0-m depth (c_r=0.74); (b) for the 11,1995–03,1996 period at 23.5-m depth (c_r=0.76); (c) for the 11,1996–03,1997 period at 15.0-m depth (c_r=0.82); (d) for the 11,1996–03,1997 period at 23.5-m depth (c_r=0.77); and (e) for the 11,1997–12,1997 period at 15.0-m depth (c_r=0.80).

each month of each year at each depth) were calculated from the hindcasted time series, separating the velocities in a positive (Northern) direction from those in a negative (Southern) direction. Taking into account possible differences for different months, these parameters were averaged for the 1958–1997 period separately for every month. These "monthly statistics" for both positive and negative directions is presented in Table 4.

The occurrence of currents in different directions (positive and negative) varies from 43% and 57% in November to 70% and 30% in January. At the same time, the dominance in magnitude of the northern currents does not vary with depth.

5.3. Extreme value statistics

Using a statistical theory of extreme values, we tried to analyze observed extremes and to forecast further possible extremes. Statistics of extremes depend upon the distribution and upon the sample size. The main question to be answered is whether a series of extreme values exhibited a regular behavior.

UNCORRECTED PROOF

ARTICLE IN PRESS

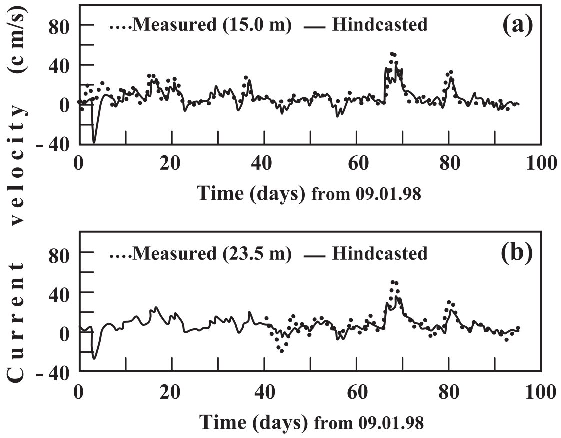

Fig. 6. Calculated and measured alongshore components of current velocity near Ashdod port: (a) for the 01,1998–03,1998 period at 15.0-m depth (c_r=0.83); and (b) for the 01,1998–03,1998 period at 23.5-m depth (c_r=0.87).

One of the best-known and widely used extreme value distributions is Weibull extreme value distribution (Gumbel, 1967). This theoretical distribution refers to maximum values measured above some threshold value, and its probability density function is given by

$$f(u) = \frac{\gamma}{\alpha}\left(\frac{u-\beta}{\alpha}\right)^{\gamma-1}\exp\left[-\left(\frac{u-\beta}{\alpha}\right)^{\gamma}\right] \quad \text{for } u > \beta \tag{16}$$

The appropriate cumulative distribution function is

$$F(u) = 1 - \exp\left[-\left(\frac{u-\beta}{\alpha}\right)^{\gamma}\right] \tag{17}$$

where γ is a shape parameter, α is a scale parameter, and β is the chosen threshold.

We compared distributions of maximum hindcasted values above some threshold with Weibull theoretical probability density functions obtained for the same series of maxima. Good agreement between theoretical and real distributions was obtained. The probability plot correlation coefficients (c_r) vary from 0.991 to 0.996 and allow one to extrapolate the possible maximum value of the alongshore component for the periods from 50 to 100 years. These maximum values can be obtained for a return period T as

$$u_{\max}^{T} = \beta + \alpha[\ln(\lambda T)]^{1/\gamma} \tag{18}$$

$\lambda = N/Y$ is the average number of observations per year, where Y is number of years of observations (Y=40 in our case), and N is total number of observations above the threshold β.

The results of this analysis are presented in Table 5 for three characteristic depths of 10, 20, and 50 m.

Table 4
Statistical parameters of the alongshore component of northern (+) and southern (−) current velocity hindcasted for the 1958–1997 period

h (m)	Month	% (+)	% (−)	$u_{\max}$ (+) (cm/s)	$u_{\max}$ (−) (cm/s)	$\bar{u}$ (+) (cm/s)	$\bar{u}$ (−) (cm/s)
1	November	44	56	41	14	15	7
	December	65	35	68	13	18	6
	January	68	32	75	15	23	8
	February	63	37	69	14	19	7
	March	60	40	57	15	16	7
10	November	43	57	33	11	11	5
	December	65	35	56	10	14	5
	January	69	31	59	10	15	5
	February	66	34	54	11	14	6
	March	65	35	50	13	13	6
20	November	45	55	29	11	9	5
	December	66	34	48	10	14	5
	January	69	31	50	10	15	4
	February	69	31	45	10	14	5
	March	69	31	40	11	14	5
50	November	51	49	24	12	9	6
	December	68	32	38	10	14	5
	January	70	30	40	11	15	5
	February	73	27	38	10	15	5
	March	77	23	36	11	14	5

Table 5
Weibull distribution parameters for different current velocities (1958–1997)

Dir	h (m)	$u_{\max}$ (cm/s)	β (cm/s)	N	α	γ	c_r	u_{50} (cm/s)	u_{100} (cm/s)
North	10	122	55	73	18.57	1.19	0.996	120	128
	20	102	50	77	14.95	1.12	0.991	99	105
	50	91	45	71	10.21	1.07	0.996	87	93
South	10	51	19	60	5.23	0.94	0.991	49	53
	20	41	14	54	4.42	0.86	0.996	37	42
	50	31	9	54	3.67	0.84	0.991	29	34

UNCORRECTED PROOF

ARTICLE IN PRESS

6. Concluding remarks

This study has tried to close an existing gap regarding the climatology of the winter currents on the Israeli Mediterranean shelf.

The authors believe that their methodology for obtaining meaningful synthetic current records from available wind and atmospheric pressure data can be used in other locations, provided that their coastlines are nearly straight and that enough measurements (needed to calibrate the friction coefficient) are available.

The relative long synthetic current records can then serve to obtain statistical averages and extreme values. Eq. (11) can, in principle, be used to obtain an estimate of v, the across-shelf-current component. However, this component is usually significantly smaller than u—the alongshore current component. The measurements of Rosentraub (1995) give $v/\bar{u}$ not larger than 20%.

In closing, we list again some of the assumptions that are embedded into the simplified mathematical model, which somewhat restrict the general applicability of this model. These limiting assumptions include (i) the constancy of the friction coefficient r; (ii) ignoring the vertical structure of the alongshore current; (iii) ignoring the deeper ocean forcing at $y=l$; and most important, (iv) the adopted dynamics omit the effect of the alongshore pressure gradient due to the differences in water surface elevations.

Note that relaxing anyone of the above assumptions would complicate the mathematical model considerably and moreover requires additional field data which were not available to us.

Acknowledgment

This work is part of a thesis by D. Kunitsa submitted to the Department of Civil Engineering, Technion-Israel Institute of Technology, in partial fulfillment of the requirements for a Doctor of Philosophy degree. M. Stiassnie acknowledges the support by the Fund for Promotion of Research at the Technion.

References

Allen, J.S., Kundu, P.K., 1978. On the momentum, vorticity and mass balance on the Oregon shelf. J. Phys. Oceanogr. 8, 13–27.

Brink, K.H., 1998. Wind-driven currents over the continental shelf. In: Brink, H., Robinson, A.R. (Eds.), The Sea, vol. 10, pp. 3–20.

Csanaday, G.T., 1978. The arrested topographic wave. J. Phys. Oceanogr. 8, 47–62.

Dean, R., Dalrymple, R., 1991. Water Wave Mechanics for Engineers and Scientists, 2nd ed. World Scientific Publishing, Singapore, 312 pp.

Gumbel, E.G., 1967. Statistics of Extremes. Columbia University Press, New York, 564 pp.

Hickey, B.M., Dobbins, E.L., Allen, S.E., 2003. Local and remote forcing of currents and temperature in the central Southern California bight. J. Geophys. Res. 108 (C3), 3081.

Jenne, R., Woollen, J., 1994. The reanalysis database, extended abstracts. Proceedings of the Tenth Conference on Numerical Weather Prediction. American Meteorological Society, Portland, OR, pp. 271–299.

Kalnay, E., Kanamitsu, M., Kistler, R., Collins, W., Deaven, D., Gandin, L., Iredell, M., Saha, S., White, G., 1996. The Ncep/NCAR 40-year reanalysis project. Bull. Am. Meteorol. Soc. 77, 437–471.

Kit, E., 1999. Current meters operation by Oceana for the 3 years period between May 1995 and July 1998, Rep. P.N. 514/99. CAMERI-Coastal and Marine Engineering research Institute, Technion, Haifa. 25 pp.

Kushnir, Y., Stiassnie, M., Kunitsa, D., Glozman, M., 2000. Extreme northerly wind storms in the Eastern Mediterranean Basin and their wave impact in deep water in Haifa Bay. 6th International Workshop on Wave Hindcasting and Forecasting. Monterey, Calif., Nov. 6–10, pp. 298–305.

Large, W.G. and S.G. Yeager, Diurnal to Decadal global forcing for ocean and sea-ice models: The data sets and flux climatologies, NCAR Technical Note TN-460+STR, 92 pp, 2004.

Lentz, S.J., Winant, C.D., 1986. Subinertial currents on the Southern California shelf. J. Phys. Oceanogr. 16, 1737–1750.

Rosentraub, Z., 1992. Study of the Circulation on the Continental Shelf of Israel, Rep. ES-25-90. IOLR-Israel Oceanographic and Limnological Research, Haifa.

Rosentraub, Z., Winter currents on the continental shelf of Israel, DSc thesis (in Hebrew, with English abstract), Technion-Israel Institute of Technology, Haifa, 1995.

UNCORRECTED PROOF